

## Supporting Information

### Rare Earth Ions Enhanced Near Infrared Fluorescence of Ag<sub>2</sub>S Quantum Dots for the Detection of Fluoride Ions in Living Cells

Caiping Ding, Xuanyu Cao, Cuiling Zhang\*, Tangrong He, Nan Hua, Yuezhong Xian,\*

\*Corresponding authors: clzhang@chem.ecnu.edu.cn; yzxian@chem.ecnu.edu.cn (Y.Z. Xian) Tel

&Fax: +86-21-54340046.

Shanghai Key Laboratory of Green Chemistry and Chemical Processes, Department of Chemistry,  
School of Chemistry and Molecular Engineering, East China Normal University, Shanghai 200241,

China

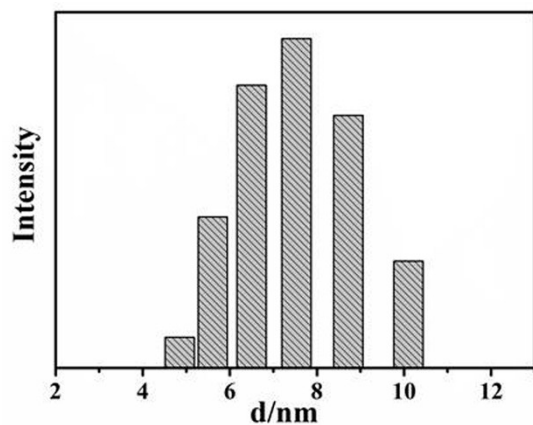


Fig. S1 The hydrodynamic size of Ag<sub>2</sub>S QDs measured by dynamic light scattering.

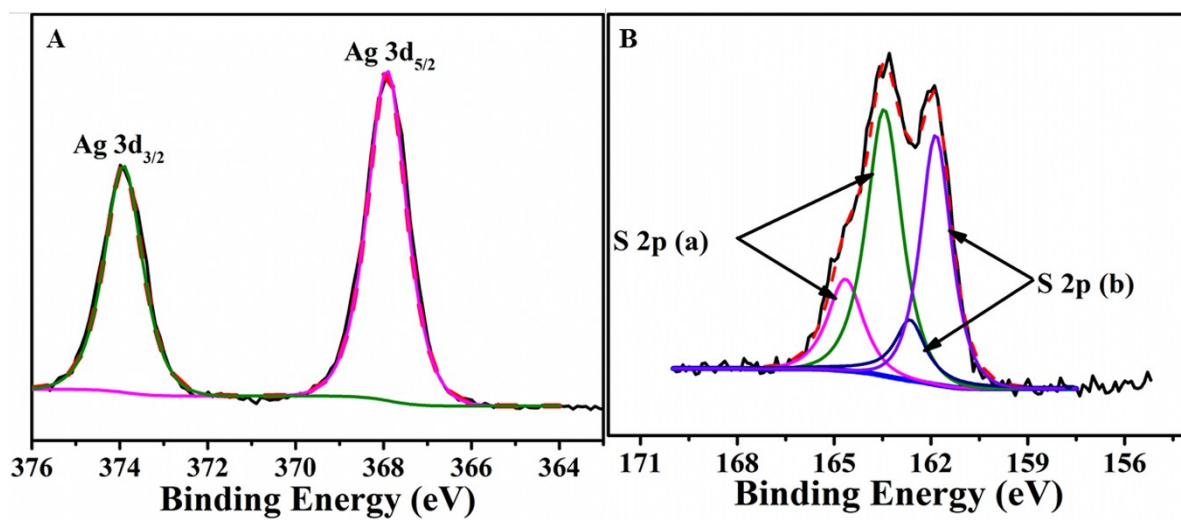
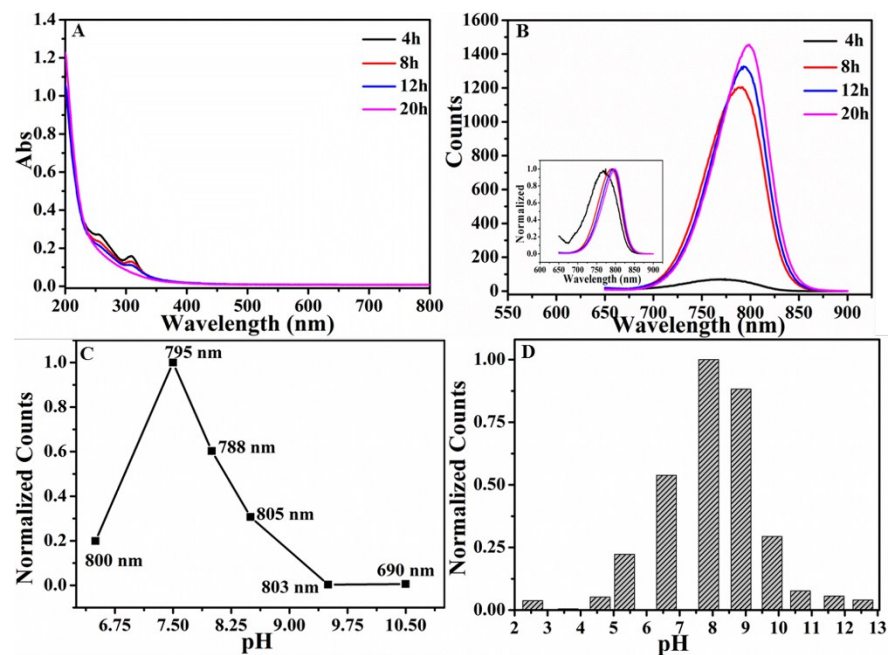
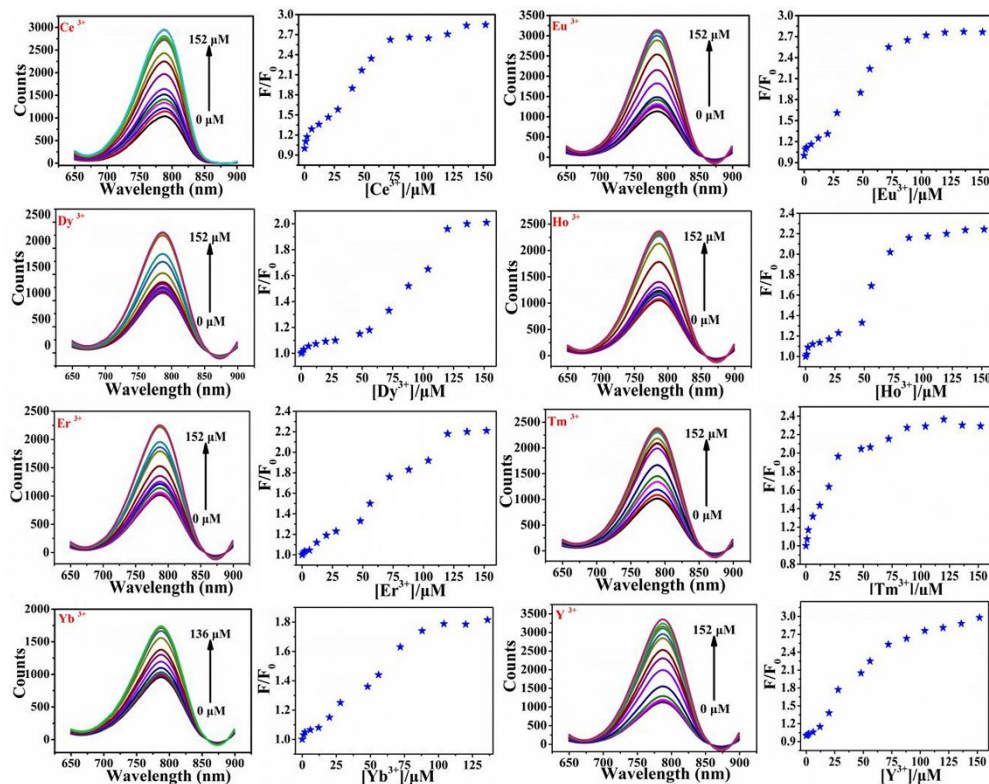


Fig. S2 XPS spectra of (A) Ag 3d and (B) S 2p for Ag<sub>2</sub>S QDs.



**Fig. S3** Absorbance (A) and fluorescence (B) spectra of the  $\text{Ag}_2\text{S}$  QDs at different reaction time, the normalized fluorescence intensity and peak position of the  $\text{Ag}_2\text{S}$  QDs at different reaction pH value (C) and (D) the pH stability toward the  $\text{Ag}_2\text{S}$  particles. Inset of (B) is the normalized fluorescence spectra.



**Fig. S4** The fluorescence intensity of  $\text{Ag}_2\text{S}$  QDs was enhanced by various trivalent rare earth ions. F and  $F_0$  are corresponding to the fluorescent intensity of  $\text{Ag}_2\text{S}$  QDs in presence or absence of rare earth ion, respectively.

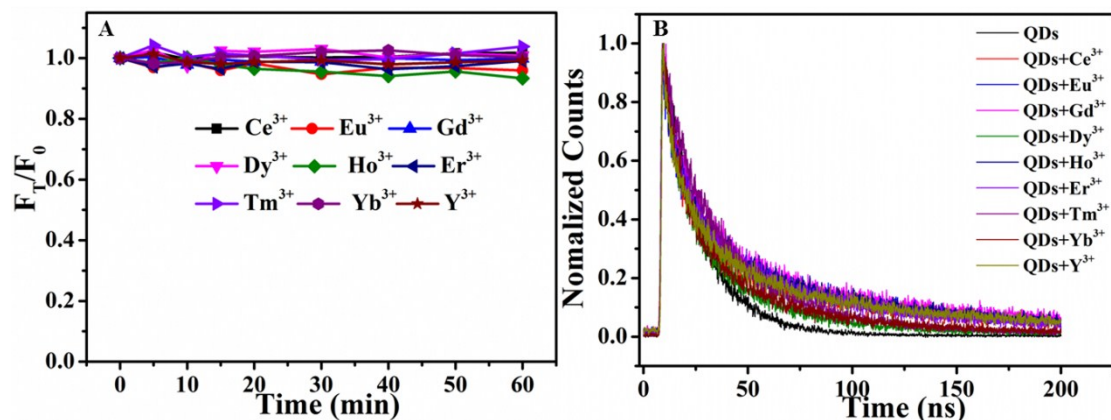


**Fig. S5** Fluorescence stability of the rare earth ions conjugated Ag<sub>2</sub>S QDs (A) and the fluorescence decay curves of QDs (B) in the absence and presence of different rare earth ions (including Ce<sup>3+</sup>, Eu<sup>3+</sup>, Gd<sup>3+</sup>, Dy<sup>3+</sup>, Ho<sup>3+</sup>, Er<sup>3+</sup>, Tm<sup>3+</sup>, Yb<sup>3+</sup> and Y<sup>3+</sup>, respectively).

**Table S1:** Zeta potential and hydrodynamic size of the Ag<sub>2</sub>S QDs colloidal in presence of different rare earth ions.

Cations	Zeta potential (mV)	Hydrodynamic size (nm)
H <sub>2</sub> O	-44.6	7.5
Gd <sup>3+</sup>	-15.5	167
Ce <sup>3+</sup>	-18.5	158
Eu <sup>3+</sup>	-23.9	142
Y <sup>3+</sup>	-26.0	129
Tm <sup>3+</sup>	-32.5	113
Ho <sup>3+</sup>	-32.8	109
Er <sup>3+</sup>	-36.5	100
Yb <sup>3+</sup>	-38.1	79
Dy <sup>3+</sup>	-39.7	60

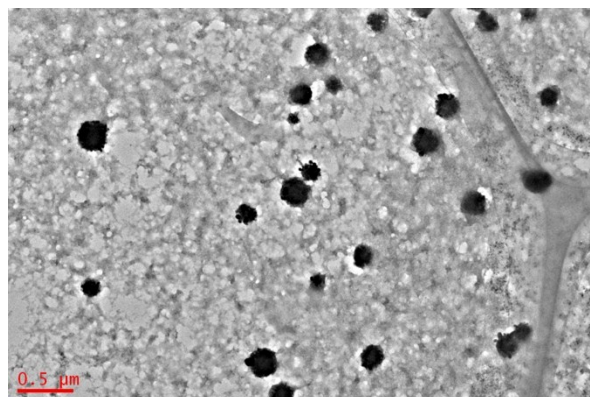


**Fig. S6** TEM images of  $\text{Ag}_2\text{S}$  QDs in the presence of  $\text{Gd}^{3+}$  (185  $\mu\text{M}$ ).

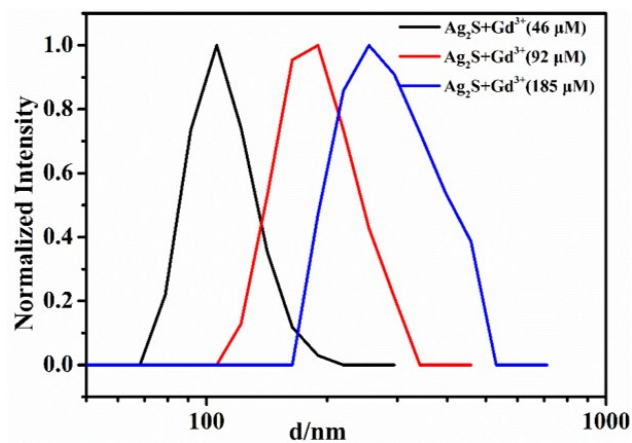


**Fig. S7** The hydrodynamic size of  $\text{Ag}_2\text{S}$  QDs with increased concentration of  $\text{Gd}^{3+}$  measured by DLS.

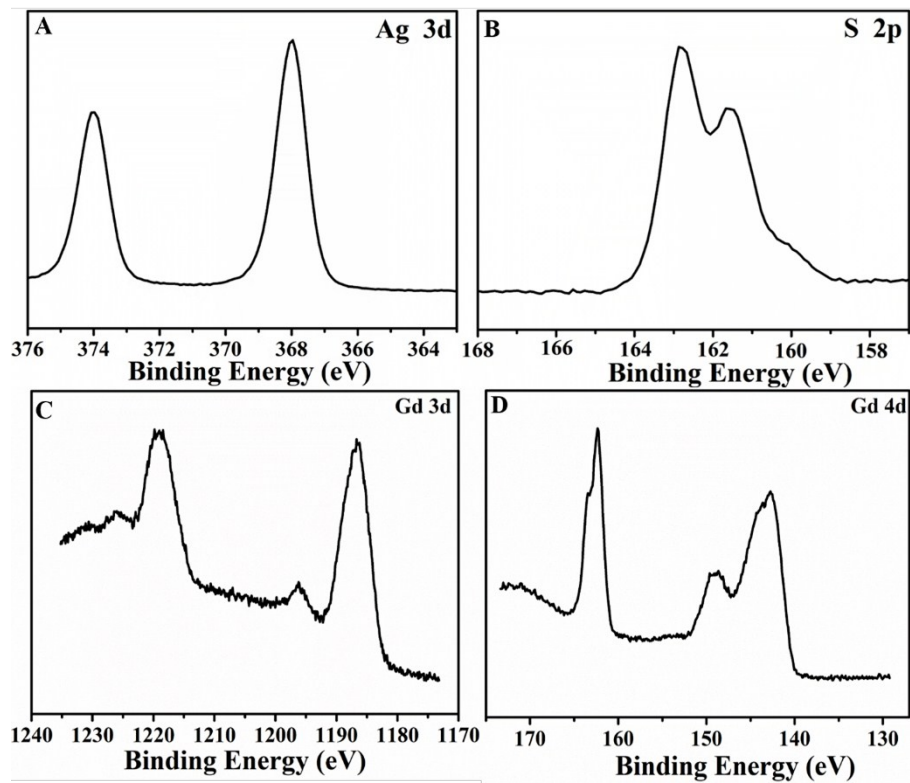


**Fig. S8** XPS spectra of  $\text{Gd}^{3+}$ - $\text{Ag}_2\text{S}$  QDs complex: (A) Ag 3d, (B) S 2p, (C) Gd 3d and Gd 4d.

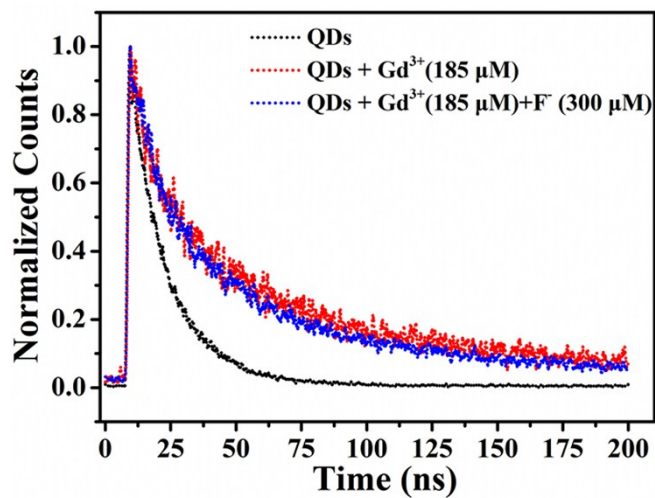


**Fig. S9** The fluorescence decay curves of  $\text{Ag}_2\text{S}$  QDs,  $\text{Ag}_2\text{S}$  QDs+ $\text{Gd}^{3+}$  (185  $\mu\text{M}$ ),  $\text{Ag}_2\text{S}$  QDs+ $\text{Gd}^{3+}$  (185  $\mu\text{M}$ ) + $\text{F}^-$  (300  $\mu\text{M}$ ).

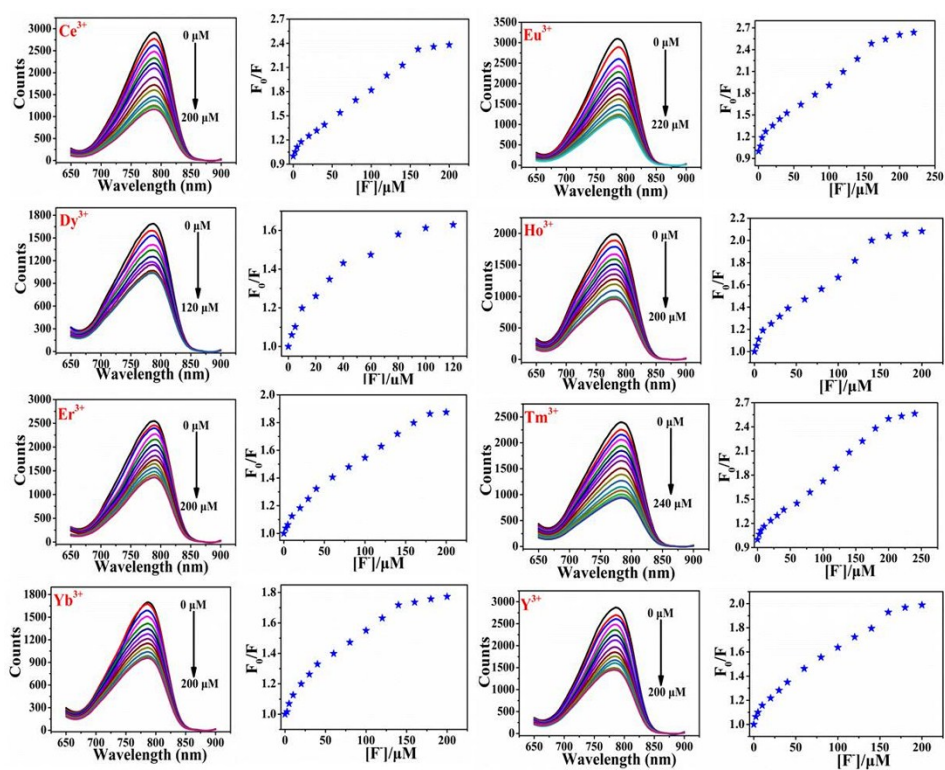


**Fig. S10** The fluorescence of rare earth ions conjugated  $\text{Ag}_2\text{S}$  QDs are quenched by  $\text{F}^-$  (left) and fluorescence response of rare earth ions conjugated  $\text{Ag}_2\text{S}$  QDs for different concentration of  $\text{F}^-$  (right), (rare earth ions =  $\text{Ce}^{3+}$ ,  $\text{Eu}^{3+}$ ,  $\text{Gd}^{3+}$ ,  $\text{Dy}^{3+}$ ,  $\text{Ho}^{3+}$ ,  $\text{Er}^{3+}$ ,  $\text{Tm}^{3+}$ ,  $\text{Yb}^{3+}$  and  $\text{Y}^{3+}$ , respectively).

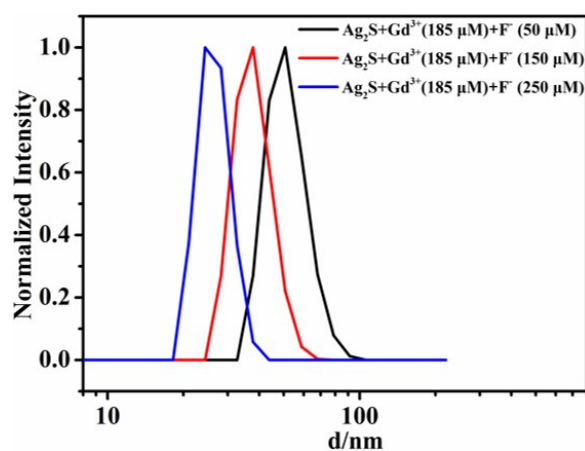


**Fig. S11** The hydrodynamic size of  $\text{Gd}^{3+}$  -  $\text{Ag}_2\text{S}$  QDs with increased concentration of  $\text{F}^-$  measured by DLS.

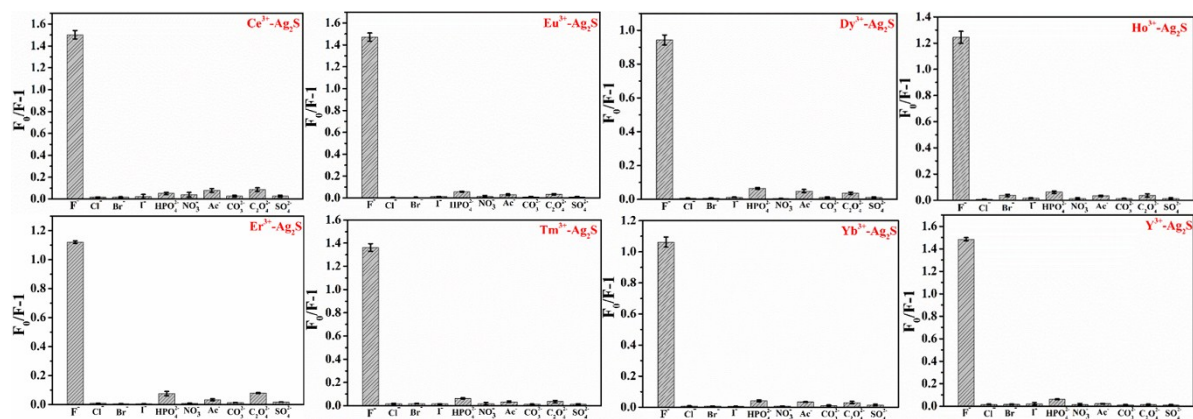


**Fig. S12** The selectivity of the rare earth ions conjugated  $\text{Ag}_2\text{S}$  QDs nanoprobe for  $\text{F}^-$  detection by monitoring the emission at 795 nm. The concentration of different anions are 250  $\mu\text{M}$ .  $F_0$  and  $F$  are the fluorescence intensity in the absence and presence of anions. (rare earth ions =  $\text{Ce}^{3+}$ ,  $\text{Eu}^{3+}$ ,  $\text{Dy}^{3+}$ ,  $\text{Ho}^{3+}$ ,  $\text{Er}^{3+}$ ,  $\text{Tm}^{3+}$ ,  $\text{Yb}^{3+}$  and  $\text{Y}^{3+}$ , respectively).

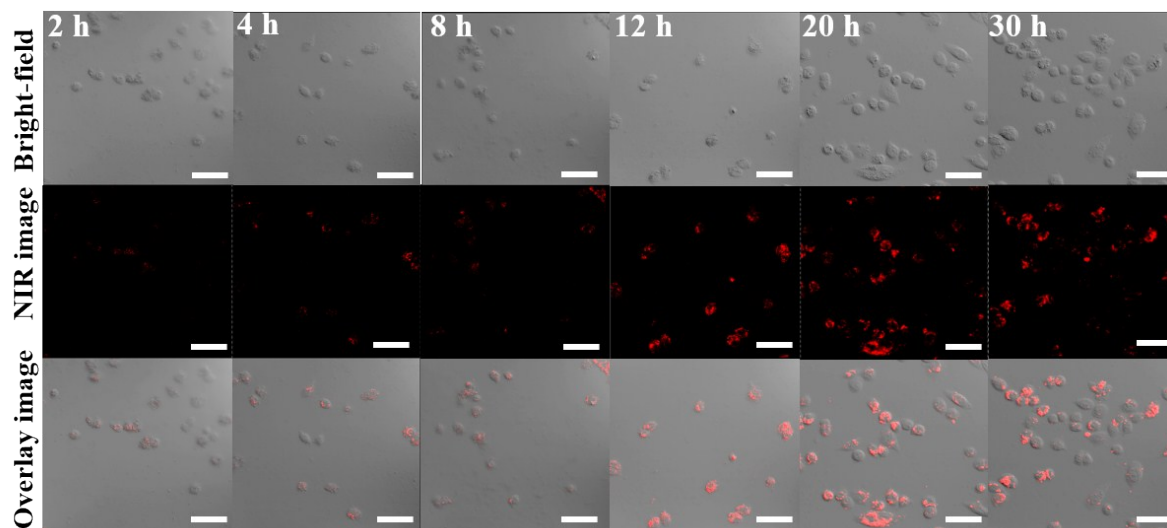


**Fig. S13** Photostability of  $\text{Gd}^{3+}$ -  $\text{Ag}_2\text{S}$  complex in MDA-MB-468 cells. The scale bar is 50  $\mu\text{m}$ .



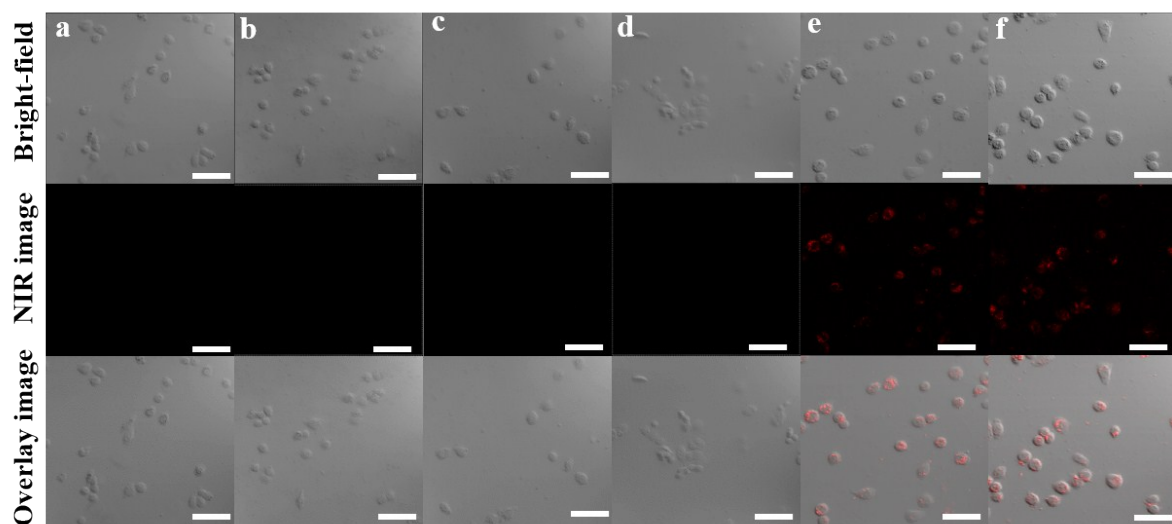


**Fig. S14** Confocal images for MDA-MB-468 cells under different conditions. (a) Control, (b) NaF (800  $\mu\text{M}$ ), (c) NaF (1600  $\mu\text{M}$ ), (d) NaF (2400  $\mu\text{M}$ ), (e)  $\text{Ag}_2\text{S}$  QDs (150  $\mu\text{g/ml}$ ), (f)  $\text{Ag}_2\text{S}$  QDs (150  $\mu\text{g/ml}$ ) and NaF (2400  $\mu\text{M}$ ). The scale bar is 50  $\mu\text{m}$ .

**Table S2:** Comparison of the sensor performance for  $\text{F}^-$  detection.

Sensor	Detection Range	Detection of limit	Ref. Our work
CuInS <sub>2</sub> QDs	0.1-700 $\mu\text{M}$	0.029 $\mu\text{M}$	[32]
$\text{Fe}_3\text{O}_4@\text{SiO}_2@\text{Carbon}$ QD	1-20 $\mu\text{M}$	0.06 $\mu\text{M}$	[29]
GO-AgNPs	0.05-0.55 nM	9.07 pM	[30]
CdTe QDs	0-10 mM	5.0 $\mu\text{M}$	[28]
CdS/ZnS nanoparticles	300-5600 $\mu\text{M}$	74.0 $\mu\text{M}$	[27]
Ag doped CdS/ZnS nanoparticles	10-1200 $\mu\text{M}$	5.25 $\mu\text{M}$	[16]
SiNWs	0.7-1.2 $\mu\text{M}$	1 $\mu\text{M}$	[34]
rare earth ion conjugated $\text{Ag}_2\text{S}$ QDs	5-260 $\mu\text{M}$	1.5 $\mu\text{M}$	Our work

**Table S3:** The detection of  $\text{F}^-$  in living cells by fluoride-ion-selective electrode (FISE) and proposed method.

Cultured $\text{F}^-$ [ $\mu\text{M}$ ]	Cells Lysates	
	$\text{F}^-$ [ $\mu\text{M}$ ] /FISE	$\text{F}^-$ [ $\mu\text{M}$ ] /proposed method
800	$92.420 \pm 0.054$	$91.579 \pm 0.011$
1600	$153.716 \pm 0.024$	$149.230 \pm 0.050$
2400	$230.865 \pm 0.034$	$229.620 \pm 0.011$